INTERNATIONAL JOURNAL FOR NUMERICAL AND ANALYTICAL METHODS IN GEOMECHANICS, VOL. 20, 307–329 (1996)

A NON-LINEAR SEISMIC RESPONSE ANALYSIS METHOD FOR SATURATED SOIL–STRUCTURE SYSTEM WITH ABSORBING BOUNDARY

T. AKIYOSHI*

Department of Civil and Environmental Engineering

H. L. FANG†

Graduate School of Science and Technology, Kumamoto University, Kurokami 2-39-1, Kumamoto 860, Japan

K. FUCHIDA‡

Department of Civil and Architectural Engineering, Yatsushiro College of Technology, Yatsushiro 866, Japan

AND

H. MATSUMOTO§

Department of Civil and Environmental Engineering, Kumamoto University, Kurokami 2-39-1, Kumamoto 860, Japan

SUMMARY

A non-linear seismic response analysis method for 2-D saturated soil–structure system with an absorbing boundary is presented. According to the 3-D strain space multimechanism model for the cyclic mobility of sandy soil, a constitutive expression for the plane strain condition is first given. Next, based on Biot's two-phase mixture theory, the finite element equations of motion for a saturated soil–structure system with an absorbing boundary during earthquake loadings are derived. A simulation of the shaking table test is performed by applying the proposed constitutive model. The effectiveness of the absorbing boundary is examined for the 2-D non-linear finite element models subjected to random inputs. Finally, a numerical seismic response analysis for a typical saturated soil–structure system is performed as an application of the proposed method.

KEY WORDS: absorbing boundary; liquefaction; saturated soil; soil–structure interaction; 3-D strain space multimechanism

INTRODUCTION

The non-linear dynamic interaction between saturated soil and structures is a very important topic in earthquake engineering as well as in structural and geotechnical engineering. The key point of this type of problem is how to model reasonably the saturated and infinite soil. Usually in order to reduce the cost of analysing this type of problem, the computational model is restricted to a finite domain with an artificial boundary. For the saturated elastic porous media, Biot's two-phase mixture theory[1] is frequently used for linear and non-linear dynamic analysis. The dynamic analysis is usually implemented via numerical methods involving discretization of both

* Professor
† Doctoral Candidate
‡ Associate Professor
§ Research Technician

CCC 0363–9061/96/050307–23

Received 8 August 1994
Revised 18 September 1994

spatial and temporal domains. The typical finite element models developed for the dynamic analysis of solid–fluid coupled problems include the work of Ghaboussi and Wilson,[2] Zienkiewicz and Shiomi,[3] Prevost,[4] Simon *et al.*[5] and Desai and Galagoda,[6] all of which account for a complex geometry and non-linear behaviour.

In the near field, the non-linear response of soil is influenced generally by various factors such as state of stress, stress path, inelasticity, volume change, and type and rate of loading. Up to now, a number of constitutive models describing the cyclic behaviour of soil have been developed.[7] Of these, the strain-space plasticity model for the cyclic mobility of sandy soil proposed by Iai *et al.*[8] appears to be practical, rational and promising. As a continuation of this model, the authors[9,10] presented the 3-D (three-dimensional) strain-space multimechanism model for the cyclic mobility of sandy soil. The constitutive properties are characterized by a volumetric mechanism and a number of microscopic simple shear mechanisms, which can take into account the effect of principal stress axis rotation.

In order to simulate the effect of the far field, it is necessary to devise special boundary techniques to incorporate the radiation condition of the truncated unbounded domain into the finite computational model. In the dynamic analysis of dry media, several techniques have been proposed. The efficient techniques are given for linear problems by the consistent boundary of Lysmer and Waas.[11] However, these methods are frequency dependent and thus inapplicable to the true non-linear analysis in the time domain. In the transient case, Lysmer and Kuhlemeyer[12] proposed the viscous boundary and Smith[13] proposed the superposition boundary to eliminate boundary reflections. Miura and Toki[14] presented a dynamic analysis method for the soil–structure system with the viscous boundary based on the principle of virtual work. In the dynamic analysis of saturated porous media, Modaressi and Benzenati[15] proposed an absorbing boundary element for the u–p formulation and presented an illustrative example of the efficiency of the proposed boundary. Degrande and Roeck[16] gave an absorbing boundary condition in the frequency domain. Recently, the authors[10,17] presented the absorbing boundary conditions in the time domain for u–w, u–U and u–p formulations. However, the work on how to model reasonably an unbounded domain in the non-linear seismic analysis of a saturated soil–structure system seems far from adequate.

In this study, a non-linear seismic response analysis method for a 2-D (two-dimensional) saturated soil–structure system with an absorbing boundary is presented. To treat non-linearity of the soil, the constitutive expression for the plane strain condition is first given according to the 3-D strain-space multimechanism model for the cyclic mobility of sandy soil proposed by the authors.[9,10] Next, based on Biot's two-phase mixture theory, the finite element equations of motion for a saturated soil–structure system with an absorbing boundary during earthquake loadings are derived. The proposed method is incorporated into the finite element program NUW2 (*n*on-linear u–w analysis in *2-dimensions*). A simulation of the shaking table test is performed by use of the proposed constitutive model. The effectiveness of the absorbing boundary is examined for 2-D non-linear finite element models subjected to random inputs. Finally, a numerical seismic response analysis for a typical saturated soil–structure system is performed. It follows that the proposed absorbing boundary condition is available even for the dynamic analysis of a non-linear saturated soil–structure system.

STRAIN-SPACE MULTIMECHANISM MODEL FOR CYCLIC MOBILITY OF SANDY SOIL

In the present analysis, the non-linear behaviour of saturated soil is treated using the strain-space multimechanism model for the cyclic mobility of sandy soil. This type of model was presented first

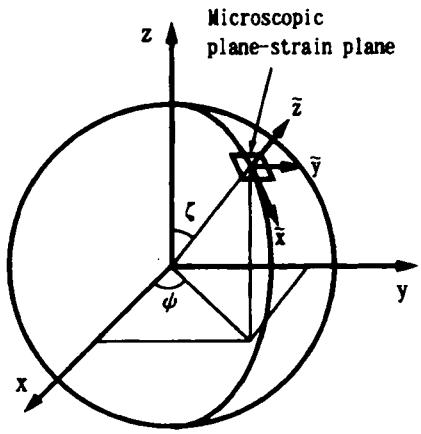

Figure 1. Local co-ordinate system associated with microscopic plane-strain plane

by Iai *et al.*[8] and modified by the authors.[9,10] Brief descriptions of the basic features of the model for the plane strain condition which is defined in the (x, z) co-ordinate plane are discussed below; more details can be found elsewhere.[9,10]

Stress–strain relationship

Sandy soil is considered to be an assemblage of particles separated by a large number of discontinuity surface (microscopic contact planes) in various orientations, which pass through the particle-to-particle contacts. For a soil mass subjected to a load, the inelastic deformations are assumed to occur mainly due to sliding, separation, and closing of the particle boundaries. Thus, around a point in the material, there may exist an infinite number of randomly oriented microscopic contact planes in space, which contribute to the inelastic deformation. It is assumed that there may exist an infinite number of randomly oriented microscopic plane-strain planes in space equivalent to the microscopic contact planes. These microscopic plane-strain planes contribute to the inelastic deformation at a point in the material. In order to describe those randomly oriented microscopic plane-strain planes, let us consider a unit sphere as shown in Figure 1. The unit vector $\tilde{\mathbf{z}}$ is normal to the arbitrary microscopic plane-strain plane on the surface of the sphere in which $\tilde{\mathbf{x}}$, $\tilde{\mathbf{y}}$ and $\tilde{\mathbf{z}}$ form a local Cartesian co-ordinate system. Expressed in terms of the angle ψ and ζ of a spherical coordinate, $\tilde{\mathbf{x}}$, $\tilde{\mathbf{y}}$ and $\tilde{\mathbf{z}}$ are given by

$$\begin{aligned}
\tilde{\mathbf{x}}^{\mathrm{T}} &= \{\cos\psi\cos\zeta,\ \sin\psi\cos\zeta,\ -\sin\zeta\} = \{l_1, m_1, n_1\} \\
\tilde{\mathbf{y}}^{\mathrm{T}} &= \{-\sin\psi,\ \cos\psi,\ 0\} = \{l_2, m_2, n_2\} \\
\tilde{\mathbf{z}}^{\mathrm{T}} &= \{\cos\psi\sin\zeta,\ \sin\psi\sin\zeta,\ \cos\zeta\} = \{l_3, m_3, n_3\}
\end{aligned} \tag{1}$$

According to the theory of microscopic model, the total deformation mechanism of soil can be decomposed into a volumetric mechanism and J sets of microscopic plane-strain shear mechanisms in various orientations. Each of these microscopic plane-strain shear mechanisms can be again decomposed into I sets of microscopic simple shear mechanisms in various orientations

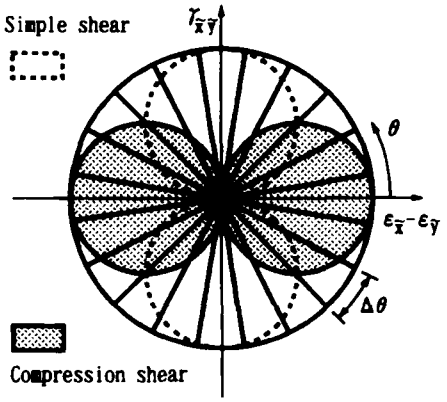

Figure 2. Microscopic simple shear mechanism

within the microscopic plane-strain plane as shown in Figure 2. By adopting J sampling plane rule,[18 19] the incremental constitutive equation is given by

$$\mathrm{d}\boldsymbol{\sigma}' = \mathbf{D}(\mathrm{d}\boldsymbol{\varepsilon} - \mathrm{d}\boldsymbol{\varepsilon}_p) \tag{2}$$

with

$$\mathbf{D} = K\mathbf{m}^{(0)}\mathbf{m}^{(0)\mathrm{T}} + 8\pi \sum_{j=1}^{J} \sum_{i=1}^{I} f^{(j)} W^{(j)} R_{\mathrm{L/U}}^{(ij)} \mathbf{m}^{(ij)} \mathbf{m}^{(ij)\mathrm{T}} \tag{3}$$

where $R_{\mathrm{L/U}}^{(ij)}$ is the microscopic tangent shear modulus for the ijth microscopic shear mechanism at loading (L) and unloading (U); $f^{(j)}$ is the distribution function of microscopic plane-strain plane directions that can introduce anisotropy of the soil in its initial state. For a statistically isotropic soil in the initial state, the distribution function is independent of the microscopic plane direction, given by $f^{(j)} = 1/(4\pi)$. $W^{(j)}$ is the weight coefficient associated with the sampling plane. The elastic tangent bulk modulus K of the soil skeleton is given approximately by

$$K = K_0(\sigma'_m/\sigma'_{m0})^{0.5} \tag{4}$$

where K_0 is the initial elastic tangent bulk modulus of the soil skeleton, which can be determined approximately by the initial elastic shear modulus G_{m0} and the Poisson's ratio ν, i.e. $K_0 = 2(1+\nu)/[3(1-2\nu)]G_{m0}$; σ'_{m0} and σ'_m are the initial and current mean effective stresses, respectively. The effective stress $\boldsymbol{\sigma}'$, the stain $\boldsymbol{\varepsilon}$ and the volumetric strain $\boldsymbol{\varepsilon}_p$ due to dilatancy are given by

$$\begin{aligned} \boldsymbol{\sigma}'^{\mathrm{T}} &= \{\sigma'_x, \sigma'_z, \tau_{zx}, \sigma'_y\} \\ \boldsymbol{\varepsilon}^{\mathrm{T}} &= \{\varepsilon_x, \varepsilon_z, \gamma_{zx}, 0\} \\ \boldsymbol{\varepsilon}_p^{\mathrm{T}} &= \{\tfrac{1}{3}\varepsilon_p, \tfrac{1}{3}\varepsilon_p, 0, \tfrac{1}{3}\varepsilon_p\} \end{aligned} \tag{5}$$

The stress direction vectors $\mathbf{m}^{(0)}$ and $\mathbf{m}^{(ij)}$ are given by

$$\mathbf{m}^{(0)\mathrm{T}} = \{1, 1, 0, 1\}$$

$$\mathbf{m}^{(ij)} = \begin{Bmatrix} (l_1^2 - l_2^2)\cos\theta_i + 2l_1 l_2 \sin\theta_i \\ (n_1^2 - n_2^2)\cos\theta_i + 2n_1 n_2 \sin\theta_i \\ (l_1 n_1 - l_2 n_2)\cos\theta_i + (l_1 n_2 + l_2 n_1)\sin\theta_i \\ (m_1^2 - m_2^2)\cos\theta_i + 2m_1 m_2 \sin\theta_i \end{Bmatrix} \tag{6}$$

where

$$\theta_i = (i - 1)\Delta\theta$$

$$\Delta\theta = \pi/I \tag{7}$$

Moreover, the integrated constitutive equation can be given by

$$\boldsymbol{\sigma}' = -B(\varepsilon_x + \varepsilon_z - \varepsilon_p)^2 \mathbf{m}^{(0)} + 8\pi \sum_{j=1}^{J} \sum_{i=1}^{I} f^{(j)} W^{(j)} Q^{(ij)}(\gamma^{(ij)}) \Delta\theta \, \mathbf{m}^{(ij)} \tag{8}$$

with

$$B = [0{\cdot}5\, K_0/(-\sigma'_{m0})^{0.5}]^2$$

$$\gamma^{(ij)} = \mathbf{m}^{(ij)\mathrm{T}} \boldsymbol{\varepsilon} \tag{9}$$

where $Q^{(ij)}$ is the microscopic shear stress per unit angle for the ijth microscopic simple shear mechanism; $\gamma^{(ij)}$ is the ijth microscopic simple shear strain.

Dilatancy model

The volumetric strain ε_p representing dilatancy is assumed to be related to the plastic shear work, which can be given by

$$\varepsilon_p = n/K_f(1 - S)\sigma'_{m0} + (1 - \sqrt{S})\sqrt{(-\sigma'_{m0})}/B \tag{10}$$

where n and K_f are the porosity of the soil skeleton and the bulk modulus of the pore water, respectively; S is the state variable, given by

$$S = S_0 \ (\text{if } r < r_3)$$

$$S = S_2 + \sqrt{(S_0 - S_2)^2 + [(r - r_3)/\sin\phi'_f]^2} \quad (\text{if } r > r_3) \tag{11}$$

with

$$r = \tau'/(-\sigma'_{m0})$$

$$\tau' = J_2'^{1/2}\left(\cos\alpha + \frac{\sqrt{3}}{2}\sin\alpha\sin\phi'_f\right)$$

$$r_2 = \sin\phi'_p S_0 \tag{12}$$

$$r_3 = 0{\cdot}67 r_2$$

$$S_2 = S_0 - (r_2 - r_3)/\sin\phi'_f$$

where ϕ'_f and ϕ'_p are the shear resistance angle and phase transformation angle, respectively; α is the angle of Lode; J'_2 is the second invariant of deviatoric effective stress tensor; S_0 is the effective stress path parameter defined by a function of normalized plastic shear work w, given by

$$\begin{aligned} S_0 &= 1 - 0{\cdot}6\,(w/w_1)^{p_1} \text{ (if } w < w_1) \\ S_0 &= (0{\cdot}4 - S_1)(w_1/w)^{p_2} + S_1 \text{ (if } w > w_1) \end{aligned} \tag{13}$$

where S_1, w_1, p_1 and p_2 are the parameters which characterize the liquefaction properties of sandy soil.

The accumulated normalized plastic shear work can be given by

$$w = W_s/(\tau_{m0}\gamma_{m0}/2) \tag{14}$$

where τ_{m0} and γ_{m0} are the drained shear strength and reference strain at the initial mean effective stress σ'_{m0}, respectively, which are defined by σ'_{m0} and the initial shear modulus G_{m0} through

$$\begin{aligned} \tau_{m0} &= -\sigma'_{m0}\sin\phi'_f \\ \gamma_{m0} &= \tau_{m0}/G_{m0} \end{aligned} \tag{15}$$

W_s is the accumulated plastic shear work, the increment of which is given approximately by

$$\mathrm{d}W_s = s'_{ij}\mathrm{d}e_{ij} - c_1|\sqrt{(J'_2)}\,\mathrm{d}(\sqrt{(J'_2)}/G_m)| \tag{16}$$

where s'_{ij} is the deviatoric effective stress tensor; $\mathrm{d}e_{ij}$ is the increment of deviatoric strain tensor; G_m is the shear modulus at the current stress state; c_1 is the parameter which characterizes no dilatancy for the cyclic shear stress or shear strain below the threshold value in the amplitude of cyclic shear stress or shear strain. Equation (16) indicates that the plastic shear work is equal to the total shear work minus the approximate elastic shear work. According to the definition of plastic shear work, $\mathrm{d}W_s$ takes a positive value or zero.

Microscopic simple shear mechanism

Now we consider the relationship of microscopic shear stress and shear strain under the cyclic loading condition. It is assumed that the memory of loading history is defined in the normalized space as shown in Figure 3, given by

$$\begin{aligned} \xi &= \gamma^{(ij)}/\gamma_v \\ \eta &= Q^{(ij)}/Q_v \end{aligned} \tag{17}$$

where ξ and η are normalized microscopic shear strain and stress, respectively, Q_v and γ_v are the microscopic shear strength and reference strain, respectively. In the above definition, the superscript (ij) is omitted from ξ and η for simplicity.

Initial loading. Based on the results of actual simple shear tests, the hyperbolic stress–strain relation is assumed approximately for the initial loading of each microscopic simple shear mechanism such as

$$Q^{(ij)} = [(\gamma^{(ij)}/\gamma_v)/(1 + |\gamma^{(ij)}/\gamma_v|)]Q_v \tag{18}$$

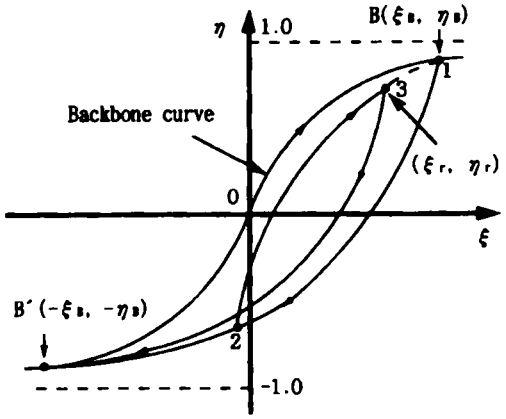

Figure 3. Loading and unloading curves in normalized space

The corresponding microscopic tangent shear modulus can be expressed as

$$R_L^{(ij)} = \frac{dQ^{(ij)}}{d\gamma^{(ij)}} \Delta\theta = [1/(1 + |\gamma^{(ij)}/\gamma_v|)^2](Q_v/\gamma_v)\Delta\theta \tag{19}$$

Unloading from initial loading. Is order to overcome the drawback that the Masing's rule cannot represent the realistic hysteresis loop when the amplitude of cyclic shear strain becomes as large as a few percent, the scaling parameters a and b for the variables ξ and η are introduced to define new variables ξ/a and η/b. When unloading begins from the initial loading, the scaling parameters a and b are used to modify the hysteresis loop which consumes a consistent amount of energy as observed in the laboratory test. According to the above method, the microscopic shear stress and shear strain relation for unloading from the initial loading may be given by

$$(Q^{(ij)}/Q_v - \eta_B)/(2b) = f[(\gamma^{(ij)}/\gamma_v - \xi_B)/(2a)] \tag{20}$$

with

$$f(\xi) = \xi/(1 + |\xi|) \tag{21}$$

where (ξ_B, η_B) is the reversal point on the back-bone curve. Then, the corresponding microscopic tangent shear modulus is obtained by

$$R_U^{(ij)} = \frac{dQ^{(ij)}}{d\gamma^{(ij)}} \Delta\theta = g[(\gamma^{(ij)}/\gamma_v - \xi_B)/(2a)](Q_v/\gamma_v)(b/a)\Delta\theta \tag{22}$$

with

$$g(\xi) = 1/(1 + |\xi|)^2 \tag{23}$$

Reloading. Similarly, the scaling parameter c for the variables ξ/a and η/b is introduced to define new variables $\xi/(ac)$ and $\eta/(bc)$ during unloading or re-unloading. Therefore, the expressions of microscopic stress and tangnet shear modulus during reloading or re-unloading may be

given, respectively, by

$$(Q^{(ij)}/Q_v - \eta_r)/(2bc) = f[(\gamma^{(ij)}/\gamma_v - \xi_r)/(2ac)] \tag{24}$$

and

$$R^{(ij)}_{L/U} = \frac{dQ^{(ij)}}{d\gamma^{(ij)}}\Delta\theta = g[(\gamma^{(ij)}/\gamma_v - \xi_r)/(2ac)](Q_v/\gamma_v)(b/a)\Delta\theta \tag{25}$$

where (ξ_r, η_r) is the most recent reversal point.

In the above equations, parameters ξ_B, η_B, ξ_r, η_r, a, b and c are separately defined for each microscopic simple shear mechanism. Parameters ξ_B, η_B, ξ_r and η_r are the internal variables determined by the memory of histories of stress and strain. Parameters Q_v, γ_v, a, b and c can be represented explicitly or implicitly by the shear modulus, shear strength and hysteretic damping factor H_m.[9,10]

FINITE ELEMENT EQUATION OF MOTION WITH ABSORBING BOUNDARY

In the seismic response analysis of the saturated soil–structure system, the computational model is restricted generally to the near field where structural embedment effects as well as geometrical irregularities can readily be considered within the framework of standard finite element modelling. The effect of the far field is taken into account in an approximate manner by imposing certain artificial boundary conditions along the interface between the near field and far field. Such boundaries are intended to satisfy the radiation condition such that reflections of waves emitting from the structure surface are somehow avoided. Based on Biot's two-phase mixture theory and the paraxial approximation, the authors[10,17] presented the absorbing boundary conditions in the time domain for u–w, u–U and u–p formulations to make the dynamic analysis of saturated porous media. By using these absorbing boundary conditions, we propose a non-linear seismic response analysis method for the saturated soil–structure system as follows.

Governing equations

Figure 4 shows a typical saturated porous soil–structure system in which the saturated soil deposit of near field occupies a domain Ω with a boundary Γ. According to Biot's two-phase mixture theory, the 2-D dynamic equilibrium equation for the soil–water phase and the generalized Darcy law for the dynamic equilibrium of the pore water can be written as[3]

$$\mathbf{L}^T\boldsymbol{\sigma} + \rho\mathbf{b} = \rho\ddot{\mathbf{u}} + \rho_f\ddot{\mathbf{w}}$$

$$-\nabla p + \rho_f\mathbf{b} = \rho_f\ddot{\mathbf{u}} + \frac{\rho_f}{n}\ddot{\mathbf{w}} + \frac{\rho_f g}{k}\dot{\mathbf{w}} \tag{26}$$

where a superposed dot indicates a time derivative and a vector matrix notation is used to represent tensors; i.e. $\boldsymbol{\sigma}^T = \{\sigma_x, \sigma_z, \tau_{zx}\}$; $\mathbf{u}^T = \{u_x, u_z\}$; $\mathbf{w}^T = \{w_x, w_z\}$; $\mathbf{b}^T = \{b_x, b_z\}$; $\nabla^T = \{\partial/\partial x, \partial/\partial z\}$ and

$$\mathbf{L}^T = \begin{pmatrix} \partial/\partial x & 0 & \partial/\partial z \\ 0 & \partial/\partial z & \partial/\partial x \end{pmatrix} \tag{27}$$

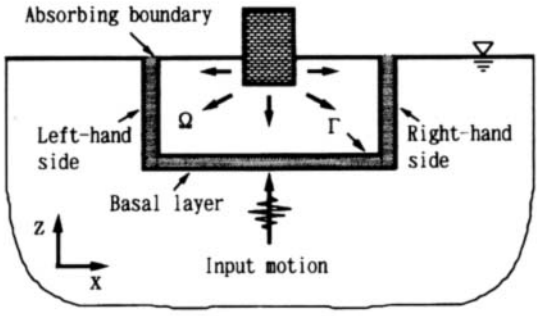

Figure 4. A typical saturated soil–structure system

Here, $\mathbf{u}$ and $\mathbf{w}$ are the soil skeleton displacement and the relative pore water displacement respectively; $\boldsymbol{\sigma}$ is the total stress; $\mathbf{b}$ is the body force per unit mass; p is the pore water pressure; ρ and ρ_f are the density of the bulk soil–water mixture and the density of the pore water, respectively, so that $\rho = (1 - n)\rho_s + n\rho_f$, where ρ_s is the density of the soil skeleton; k is the isotropic permeability coefficient and n is the porosity of the soil.

For compressible water, the stress–strain relationship can be written as

$$\mathrm{d}\boldsymbol{\sigma} = \mathrm{d}\boldsymbol{\sigma}' - \alpha\mathbf{m}\,\mathrm{d}p = \mathbf{D}\,\mathrm{d}\boldsymbol{\varepsilon} - \alpha\mathbf{m}\,\mathrm{d}p$$

$$p = -\alpha Q\mathbf{m}^{\mathrm{T}}\boldsymbol{\varepsilon} - Q\zeta_f \tag{28}$$

where $\mathbf{m}^{\mathrm{T}} = \{1, 1, 0\}$ is equivalent to the Kronecker's delta; $\boldsymbol{\sigma}'$ and $\boldsymbol{\varepsilon}$ are the effective stress and strain in the soil, respectively, given by $\boldsymbol{\sigma}'^{\mathrm{T}} = \{\sigma_x', \sigma_z', \tau_{zx}\}$ and $\boldsymbol{\varepsilon}^{\mathrm{T}} = \{\varepsilon_x, \varepsilon_z, \gamma_{zx}\}$; $\mathbf{D}$ is the stiffness matrix defined by equation (3); α and Q are Biot's constants in which $\alpha = 1$ and $Q = K_f/n$ are taken as approximate for the saturated soil; ζ_f is the volumetric strain in the pore water.

The small strain–displacement relation can be written as

$$\boldsymbol{\varepsilon} = \mathbf{L}\mathbf{u}$$

$$\zeta_f = \nabla^{\mathrm{T}}\mathbf{w} \tag{29}$$

Boundary conditions

Three types of boundary condition on the boundary Γ can be considered.

The natural boundary conditions are

$$\boldsymbol{\sigma}\mathbf{n} - \hat{\mathbf{t}} = \mathbf{0} \quad \text{on } \Gamma_\sigma$$

$$(\hat{p} - p)\mathbf{n} = \mathbf{0} \quad \text{on } \Gamma_p \tag{30}$$

where $\hat{\mathbf{t}}$ and $\hat{p}$ are the traction on the boundary Γ_p and the pore water pressure on the boundary Γ_p, respectively; $\mathbf{n}$ is the direction cosine vector on the boundary.

The essential boundary conditions are

$$\mathbf{u} - \hat{\mathbf{u}} = \mathbf{0} \quad \text{on } \Gamma_u$$

$$\mathbf{w} - \hat{\mathbf{w}} = \mathbf{0} \quad \text{on } \Gamma_w \tag{31}$$

Besides the above two types of boundary conditions, an absorbing boundary Γ_a is considered. On Γ_a, an absorbing boundary condition in the time domain is used which approximately models the radiation of waves in an unbounded space domain. A 2-D absorbing boundary condition for the u–w formulation has been established in a local $(\tilde{x}, \tilde{z})$ Cartesian co-ordinate system where $\tilde{z}$ and $\tilde{x}$ are normal (in the direction of the outward normal $\mathbf{n}$) and tangential to the boundary, respectively. The absorbing boundary condition establishes a relation between stresses and displacements, and can be considered as a mixed boundary condition, i.e.

$$\{\tilde{\tau}_{zx}, \tilde{\sigma}_z, 0, -\tilde{p}\}^{\mathrm{T}} = -\begin{pmatrix} \mathbf{A}_{uu} & \mathbf{A}_{uw} \\ \mathbf{A}_{uw}^{\mathrm{T}} & \mathbf{A}_{ww} \end{pmatrix} \begin{Bmatrix} \dot{\tilde{u}} \\ \dot{\tilde{w}} \end{Bmatrix} \tag{32}$$

with

$$\mathbf{A}_{uu} = \begin{pmatrix} \rho V_s & 0 \\ 0 & \rho V_p \end{pmatrix}; \qquad \mathbf{A}_{uw} = \begin{pmatrix} 0 & 0 \\ 0 & \alpha Q/V_p \end{pmatrix}$$

$$\mathbf{A}_{ww} = \begin{pmatrix} 0 & 0 \\ 0 & Q/V_p \end{pmatrix} \tag{33}$$

$$V_p = \sqrt{[(\lambda + 2G + \alpha^2 Q)/\rho]}; \qquad V_s = \sqrt{G/\rho}$$

where λ and G are the Lamé's constants and G is also called the shear modulus.

As the absorbing boundary condition is defined in a local $(\tilde{x}, \tilde{z})$ Catresian co-ordinate system, a co-ordinate transformation from the local $(\tilde{x}, \tilde{z})$ to the global (x, z) Cartesian co-ordinate system is needed. Hence, a projection matrix $\mathbf{P}$ which relates a vector $\tilde{v}$ given in the local Cartesian co-ordinate system on the absorbing boundary to the global Cartesian co-ordinate system $\mathbf{v}$ is defined as

$$\tilde{\mathbf{v}} = \mathbf{P}\mathbf{v} \tag{34}$$

By using the projection matrix $\mathbf{P}$ for equation (32) and considering the motion of the free field during earthquake, the absorbing boundary condition in the global Cartesian co-ordinate system can be given by

$$\begin{Bmatrix} \hat{\mathbf{t}} \\ -\hat{p}\mathbf{n} \end{Bmatrix} = \begin{Bmatrix} \hat{\mathbf{t}}^f \\ -\hat{p}^f\mathbf{n} \end{Bmatrix} - \begin{pmatrix} \mathbf{P}^{\mathrm{T}}\mathbf{A}_{uu}\mathbf{P} & \mathbf{P}^{\mathrm{T}}\mathbf{A}_{uw}\mathbf{P} \\ \mathbf{P}^{\mathrm{T}}\mathbf{A}_{uw}^{\mathrm{T}}\mathbf{P} & \mathbf{P}^{\mathrm{T}}\mathbf{A}_{ww}\mathbf{P} \end{pmatrix} \begin{Bmatrix} \dot{u} - \dot{u}^f \\ \dot{w} - \dot{w}^f \end{Bmatrix} \tag{35}$$

where a superscript f on a variable represents the contribution from the motion of the free field.

The parts Γ_σ, Γ_p, Γ_u, Γ_w and Γ_a of the boundary Γ on which the natural, essential and mixed boundary conditions are specified to satisfy the following conditions:

$$\overline{\Gamma_\sigma \cup \Gamma_p \cup \Gamma_u \cup \Gamma_w \cup \Gamma_a} = \Gamma$$

$$\Gamma_u \cap \Gamma_\sigma = 0; \qquad \Gamma_u \cap \Gamma_a = 0; \qquad \Gamma_\sigma \cap \Gamma_a = 0$$

$$\Gamma_w \cap \Gamma_p = 0; \qquad \Gamma_w \cap \Gamma_a = 0; \qquad \Gamma_p \cap \Gamma_a = 0; \tag{36}$$

Irreducible weak Galerkin formulation with absorbing boundary

In an irreducible u–w formulation for compressible water, the dynamic behaviour of the saturated porous medium occupying a domain Ω with a boundary Γ is described by the

equilibrium and boundary equations. Satisfying these equations is equivalent to the following integral equation:

$$\int_\Omega \delta\mathbf{u}^T[\mathbf{L}^T\boldsymbol{\sigma} + \rho\mathbf{b} - \rho\ddot{\mathbf{u}} - \rho_f\ddot{\mathbf{w}}]\,d\Omega + \int_{\Gamma_\sigma} \delta\hat{\mathbf{u}}^T(\boldsymbol{\sigma}\mathbf{n} - \hat{\mathbf{t}})\,d\Gamma + \int_{\Gamma_\sigma} \delta\hat{\mathbf{u}}^T(\boldsymbol{\sigma}\mathbf{n} - \hat{\mathbf{t}})\,d\Gamma = 0 \tag{37}$$

$$\int_\Omega \delta\mathbf{w}^T\left[-\nabla p + \rho_f\mathbf{b} - \frac{\rho_f g}{k}\dot{\mathbf{w}} - \rho_f\ddot{\mathbf{u}} - \frac{\rho_f}{n}\ddot{\mathbf{w}}\right]d\Omega$$

$$+ \int_{\Gamma_p} \delta\hat{\mathbf{w}}^T(\hat{p} - p)\mathbf{n}\,d\Gamma + \int_{\Gamma_\sigma} \delta\hat{\mathbf{w}}^T(\hat{p} - p)\mathbf{n}\,d\Gamma = 0$$

where the virtual displacements $\delta\mathbf{u}$, $\delta\hat{\mathbf{u}}$, $\delta\mathbf{w}$ and $\delta\hat{\mathbf{w}}$ satisfy the essential boundary conditions. The particular choice of these virtual displacements leads to a Galerkin formulation. The total stress σ and the pore fluid pressure p are enforced through natural boundary conditions. A weak Galerkin formulation can be obtained by the application of Green's theorem for integration by parts on the terms containing $\mathbf{L}^T\sigma$ and ∇p;

$$-\int_\Omega \delta\boldsymbol{\varepsilon}^T\boldsymbol{\sigma}\,d\Omega + \int_\Gamma \delta\boldsymbol{\sigma}\mathbf{n}\,d\Gamma + \int_\Omega \delta\mathbf{u}^T[\rho\mathbf{b} - \rho\ddot{\mathbf{u}} - \rho_f\ddot{\mathbf{w}}]\,d\Omega + \int_{\Gamma_\sigma} \delta\hat{\mathbf{u}}^T(\boldsymbol{\sigma}\mathbf{n} - \hat{\mathbf{t}})\,d\Gamma + \int_{\Gamma_\sigma} \delta\hat{\mathbf{u}}^T(\boldsymbol{\sigma}\mathbf{n} - \hat{\mathbf{t}})\,d\Gamma = 0$$

$$\int_\Omega \delta\zeta_f p\,d\Omega - \int_\Gamma \delta\mathbf{w}^T p\mathbf{n}\,d\Gamma + \int_\Omega \delta\mathbf{w}^T\left[\rho_f\mathbf{b} - \frac{\rho_f g}{k}\dot{\mathbf{w}} - \rho_f\ddot{\mathbf{u}} - \frac{\rho_f}{n}\ddot{\mathbf{w}}\right]d\Omega \tag{38}$$

$$+ \int_{\Gamma_p} \delta\hat{\mathbf{w}}^T(\hat{p} - p)\mathbf{n}\,d\Gamma + \int_{\Gamma_\sigma} \delta\hat{\mathbf{w}}^T(\hat{p} - p)\mathbf{n}\,d\Gamma = 0$$

As the virtual displacements are arbitrary, we can choose $\delta\hat{\mathbf{u}} = -\delta\mathbf{u}$ and $\delta\hat{\mathbf{w}} = -\delta\mathbf{w}$. The virtual displacements $\delta\mathbf{u}$ and $\delta\mathbf{w}$ fulfill the essential boundary conditions on the part of the boundary Γ where no natural or mixed boundary conditions are specified. Therefore, equation (38) becomes the following virtual expression:

$$\int_\Omega \delta\boldsymbol{\varepsilon}^T\boldsymbol{\sigma}\,d\Omega - \int_\Omega \delta\mathbf{u}^T[\rho\mathbf{b} - \rho\ddot{\mathbf{u}} - \rho_f\ddot{\mathbf{w}}]\,d\Omega - \int_{\Gamma_\sigma} \delta\hat{\mathbf{u}}^T\hat{\mathbf{t}}\,d\Gamma - \int_{\Gamma_\sigma} \delta\hat{\mathbf{u}}^T\hat{\mathbf{t}}\,d\Gamma = 0$$

$$-\int_\Omega \delta\zeta_f p\,d\Omega - \int_\Omega \delta\mathbf{w}^T\left[\rho_f\mathbf{b} - \frac{\rho_f g}{k}\dot{\mathbf{w}} - \rho_f\ddot{\mathbf{u}} - \frac{\rho_f}{n}\ddot{\mathbf{w}}\right]d\Omega + \int_{\Gamma_p} \delta\hat{\mathbf{w}}^T\hat{p}\mathbf{n}\,d\Gamma + \int_{\Gamma_\sigma} \delta\hat{\mathbf{w}}^T\hat{p}\mathbf{n}\,d\Gamma = 0 \tag{39}$$

where the last integrals on the left-hand side of equation (39) are the contributions of the absorbing boundary.

Formulation of finite element with absorbing boundary

In a finite element formulation, the spatial approximations are given by

$$\mathbf{u} = \mathbf{N}_u\bar{\mathbf{u}}$$
$$\mathbf{w} = \mathbf{N}_w\bar{\mathbf{w}} \tag{40}$$

where $\mathbf{N}_u$ and $\mathbf{N}_w$ are the shape functions for the soil skeleton and pore water displacements, respectively; $\bar{\mathbf{u}}$ and $\bar{\mathbf{w}}$ are the nodal displacements. The introduction of the approximation in the

integral statement in equation (39) can be considered as a weighted residual statement. As this statement must hold for any virtual nodal displacements $\delta\mathbf{u}$ and $\delta\mathbf{w}$, the matrix form of the irreducible weak Galerkin formulation for a saturated porous medium with compressible pore water during earthquake loadings, including an absorbing boundary condition, can be written as

$$\begin{pmatrix} \mathbf{m}_{uu} & \mathbf{m}_{uw} \\ \mathbf{m}_{uw}^{\mathrm{T}} & \mathbf{m}_{ww} \end{pmatrix} \begin{Bmatrix} \ddot{\mathbf{u}} \\ \ddot{\mathbf{w}} \end{Bmatrix} + \begin{pmatrix} 0 & 0 \\ 0 & \mathbf{c}_{ww} \end{pmatrix} \begin{Bmatrix} \dot{\mathbf{u}} \\ \dot{\mathbf{w}} \end{Bmatrix} + \begin{pmatrix} \mathbf{k}_{uu} & \mathbf{k}_{uw} \\ \mathbf{k}_{uw}^{\mathrm{T}} & \mathbf{k}_{ww} \end{pmatrix} \begin{Bmatrix} \bar{\mathbf{u}} \\ \bar{\mathbf{w}} \end{Bmatrix}$$
$$+ \begin{Bmatrix} \int_{\Omega} \mathbf{B}_u^{\mathrm{T}} \boldsymbol{\sigma}' \, \mathrm{d}\Omega \\ 0 \end{Bmatrix} = \begin{Bmatrix} \bar{\mathbf{f}}_u + \bar{\mathbf{f}}_u^f \\ \bar{\mathbf{f}}_w + \bar{\mathbf{f}}_w^f \end{Bmatrix} + \begin{pmatrix} \mathbf{c}'_{uu} & \mathbf{c}'_{uw} \\ \mathbf{c}'^{\mathrm{T}}_{uw} & \mathbf{c}'_{ww} \end{pmatrix} \begin{Bmatrix} \dot{\bar{\mathbf{u}}}^f - \dot{\bar{\mathbf{u}}} \\ \dot{\bar{\mathbf{w}}}^f - \dot{\bar{\mathbf{w}}} \end{Bmatrix} \tag{41}$$

with

$$\mathbf{m}_{uu} = \int_{\Omega} \mathbf{N}_u^{\mathrm{T}} \rho \mathbf{N}_u \, \mathrm{d}\Omega; \qquad \mathbf{m}_{uw} = \int_{\Omega} \mathbf{N}_u^{\mathrm{T}} \rho_f \mathbf{N}_w \, \mathrm{d}\Omega$$

$$\mathbf{m}_{ww} = \int_{\Omega} \mathbf{N}_w^{\mathrm{T}} (\rho_f / n) \mathbf{N}_w \, \mathrm{d}\Omega; \qquad \mathbf{c}_{ww} = \int_{\Omega} \mathbf{N}_w^{\mathrm{T}} (\rho_f g / k) \mathbf{N}_w \, \mathrm{d}\Omega$$

$$\mathbf{c}'_{uu} = \int_{\Gamma_e} \mathbf{N}_u^{\mathrm{T}} \mathbf{P}^{\mathrm{T}} \mathbf{A}_{uu} \mathbf{P} \mathbf{N}_u \, \mathrm{d}\Gamma; \qquad \mathbf{c}'_{uw} = \int_{\Gamma_e} \mathbf{N}_u^{\mathrm{T}} \mathbf{P}^{\mathrm{T}} \mathbf{A}_{uw} \mathbf{P} \mathbf{N}_w \, \mathrm{d}\Gamma$$

$$\mathbf{c}'_{ww} = \int_{\Gamma_e} \mathbf{N}_u^{\mathrm{T}} \mathbf{P}^{\mathrm{T}} \mathbf{A}_{ww} \mathbf{P} \mathbf{N}_w \, \mathrm{d}\Gamma; \qquad \mathbf{k}_{uu} = \int_{\Omega} \mathbf{B}_u^{\mathrm{T}} \alpha^2 \mathbf{Q} \mathbf{m} \mathbf{m}^{\mathrm{T}} \mathbf{B}_u \, \mathrm{d}\Omega \tag{42}$$

$$\mathbf{k}_{uw} = \int_{\Omega} \mathbf{B}_u^{\mathrm{T}} \alpha Q \mathbf{m} \mathbf{B}_w \, \mathrm{d}\Omega; \qquad \mathbf{k}_{ww} = \int_{\Omega} \mathbf{B}_w^{\mathrm{T}} Q \mathbf{B}_w \, \mathrm{d}\Omega$$

$$\bar{\mathbf{f}}_u = \int_{\Omega} \mathbf{N}_u^{\mathrm{T}} \rho \mathbf{b} \, \mathrm{d}\Omega + \int_{\Gamma_e} \mathbf{N}_u^{\mathrm{T}} \hat{\mathbf{t}} \, \mathrm{d}\Gamma; \qquad \bar{\mathbf{f}}_w = \int_{\Omega} \mathbf{N}_w^{\mathrm{T}} \rho_f \mathbf{b} \, \mathrm{d}\Omega - \int_{\Gamma_e} \mathbf{N}_w^{\mathrm{T}} \hat{p} \mathbf{n} \, \mathrm{d}\Gamma;$$

$$\bar{\mathbf{f}}_u^f = \int_{\Gamma_e} \mathbf{N}_u^{\mathrm{T}} \hat{\mathbf{t}}^f \, \mathrm{d}\Gamma; \qquad \bar{\mathbf{f}}_w^f = -\int_{\Gamma_e} \mathbf{N}_w^{\mathrm{T}} \hat{p}^f \mathbf{n} \, \mathrm{d}\Gamma$$

where $\mathbf{c}'_{uu}$, $\mathbf{c}'_{uw}$ and $\mathbf{c}'_{ww}$ are the viscous boundary matrices contributed by the absorbing boundary; $\mathbf{B}_u$ and $\mathbf{B}_w$ are the strain matrices of the soil skeleton and the pore water, respectively; $\bar{\mathbf{f}}_u^f$ and $\bar{\mathbf{f}}_w^f$ are the equivalent nodal forces corresponding to the stresses on the absorbing boundary due to the motion of the free field in the outer domain.

Since the absorbing boundary condition is derived for a linear material and some assumptions are taken in the derivation, equation (32) is appropriate for linear material in principle and approximate. For non-linear material, equation (32) is also considered as an approximation. Hence, in order to determine the viscous boundary matrices $\mathbf{c}'_{uu}$, $\mathbf{c}'_{uw}$ and $\mathbf{c}'_{ww}$ in equation (41), λ and G in equation (33) need to be assigned the current values because they will change at every time step in the non-linear computation. Similarly, $\bar{\mathbf{f}}_u^f$, $\bar{\mathbf{f}}_w^f$, $\dot{\bar{\mathbf{u}}}^f$ and $\dot{\bar{\mathbf{w}}}^f$ in equation (41) are determined by non-linear dynamic analysis of the free field in the outer domain. It is pointed that the earthquake wave in the free field is given at its bottom boundary. For this case, it is not difficult to make non-linear dynamic analysis of the free field. If the earthquake wave is given at the free surface, a deconvolution analysis is needed and may be not easy task for the non-linear case. But, this problem is out of the scope of the present paper.

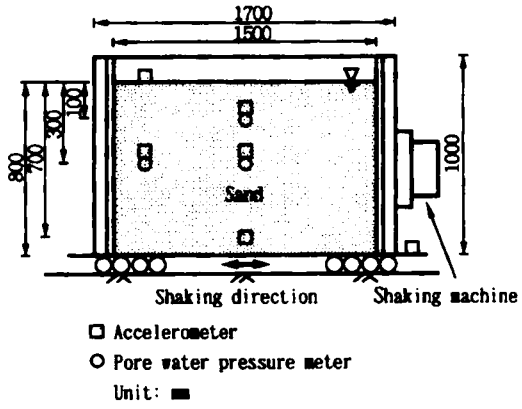

Figure 5. Setup of model test

VALIDATION OF PROPOSED METHOD

In order to verify the accuracy and efficiency of the proposed constitutive model and the absorbing boundary condition for the analysis of the saturated soil–structure system, a numerical simulation of the shaking table test and seismic response analyses of saturated soil deposits are performed. The proposed method is incorporated into the finite element program NUW2. In calculations, the four-node bilinear isoparametric element, the Newmark integration scheme and the Newton–Ralphson type iterative procedure are used. It is well known in dynamic analysis that some choices of the parameters occurring in the Newmark algorithm while preserving stability allow numerical oscillation to continue. Others, by introducing a small numerical damping, give essentially more accurate results. Hence, the Newmark parameters are chosen as $\gamma = 0{\cdot}60$ and $\beta = 0{\cdot}3025$ to maximize high-frequency numerical dissipation.[3,4]

Simulation of shaking table test

We first perform a simulation of the shaking table test by use of the proposed constitutive model. The test model of saturated sandy soil deposits is shown in Figure 5. The input motion used in the test is a sinusoidal wave with a frequency of 5 Hz and a maximum acceleration of about 0·13 g. Based on the parameter calibration procedure described in Reference 9, the soil parameters for the analysis are given as: $G_{m0} = 63{,}154$ kPa, in which G_{m0} is the initial shear modulus at $\sigma'_{m0} = -98$ kPa; $\nu = 0{\cdot}35$; $\phi'_f = 37°$; $\phi'_p = 30°$; $p_1 = 0{\cdot}5$; $p_2 = 1{\cdot}3$; $w_1 = 4{\cdot}2$; $S_1 = 0{\cdot}005$; $c_1 = 1{\cdot}5$; $n = 0{\cdot}45$; $\rho = 2{\cdot}0$ t/m^3; $\rho_f = 1{\cdot}0$ t/m^3; $k = 1{\cdot}38 \times 10^{-4}$ m/s; $H_m = 0{\cdot}3$; $\alpha = 1{\cdot}0$; $K_f = 2{\cdot}0 \times 10^6$ kPa. A 2-D analysis is performed with the repeating side boundaries,[3,6] in which displacements of the side boundary nodes on the same horizontal planes are considered to be the same in order to simulate the shear box condition. Moreover, a small Rayleigh damping ($\alpha_d = 0$ and $\beta_d = 0{\cdot}005$) which is proportionally decreasing with the degree of cyclic mobility is used to ensure the stability of the numerical solution process because the modulus of soil is very small near to liquefaction.

Figure 6 shows a comparison between the measured and computed excess pore water pressures and horizontal accelerations at a depth of 300 mm. The computed excess pore water pressure agrees well with the experimental result. Moreover, although the computed horizontal acceleration after liquefaction is larger than the measured value, the same tendency in the time history is

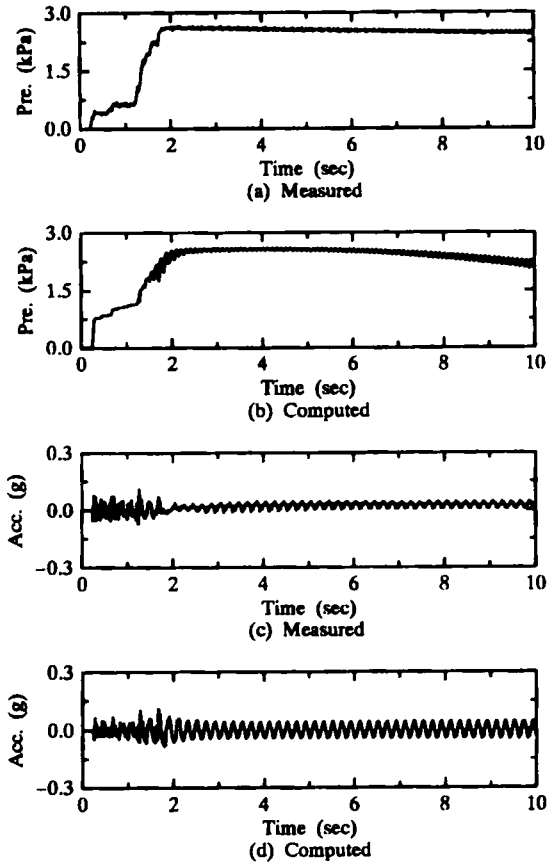

Figure 6. Acceleration and excess pore water pressure at depth of 300 mm

exhibited by both measured and computed results. These show that the proposed constitutive equation is capable of modelling the liquefaction behaviour of sandy soil.

Seismic response analyses of saturated soil deposits

To investigate the efficiency of the proposed absorbing boundary condition for seismic response analyses of saturated soil deposits, a 2-D finite element model (2-D site model) of the saturated soil deposits is presented as shown in Figure 7(a), in which both side boundaries are chosen as the proposed absorbing boundaries and the bottom boundary is assumed to be rigid and impervious. Also, the shear column of 5 two-dimensional plane elements (2-D shear column) with the repeating side boundaries and the same bottom boundary used in the 2-D site model, as shown in Figure 7(b), is prepared for the absorbing boundary condition as the far field model and used as the reference model. In numerical analyses, the motion of the El Centro Earthquake (1940 NS) with the maximum acceleration of 0·2 g is applied horizontally at the bottom boundaries of the two models. If the absorbing boundary is not very efficient, there may exist differences between the results computed by the 2-D site model and shear column. Hence, the validity of the proposed absorbing boundary will be evaluated by the differences between both responses.

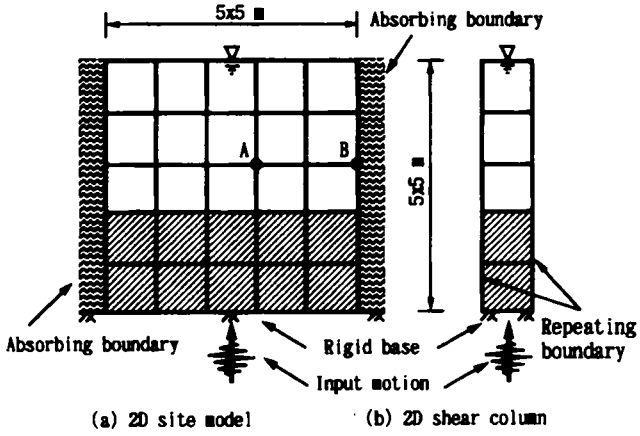

Figure 7. A saturated soil deposit

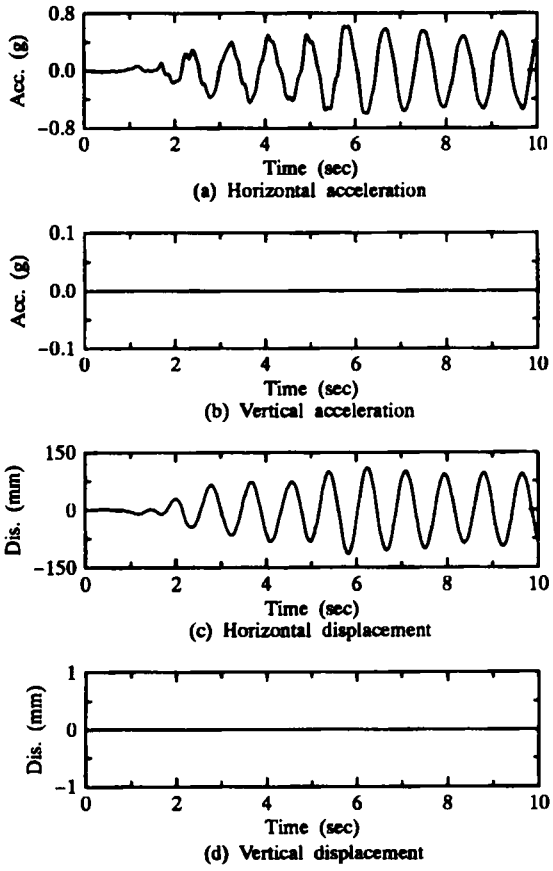

Figure 8. Seismic responses of 2-D shear column

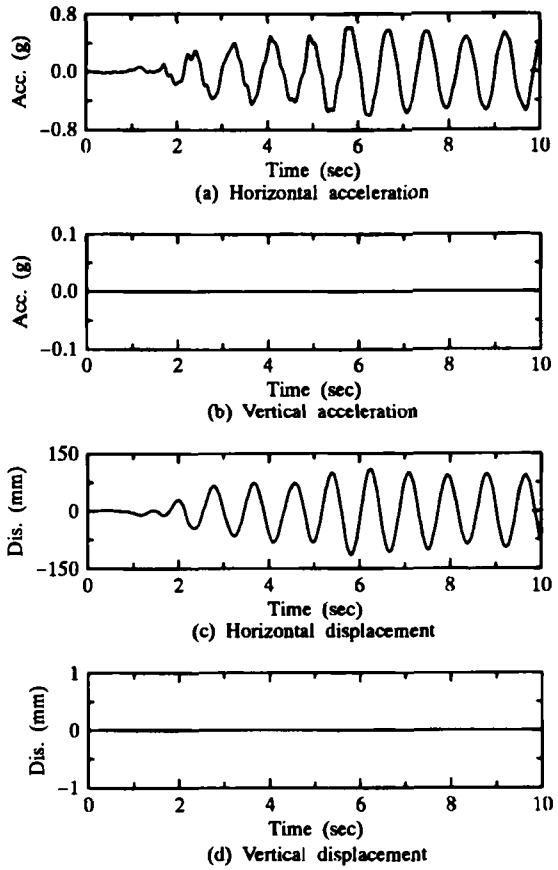

Figure 9. Seismic responses of 2-D site model with lateral absorbing boundaries

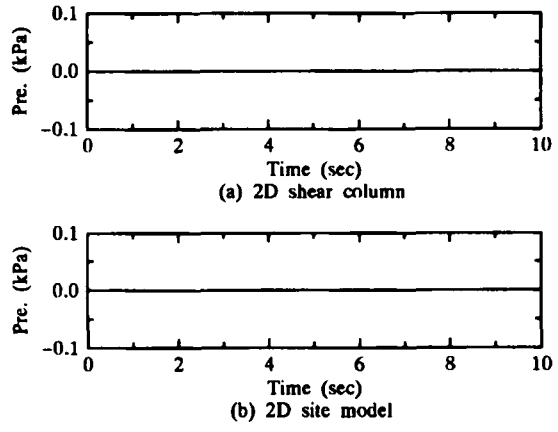

Figure 10. Excess pore water pressures

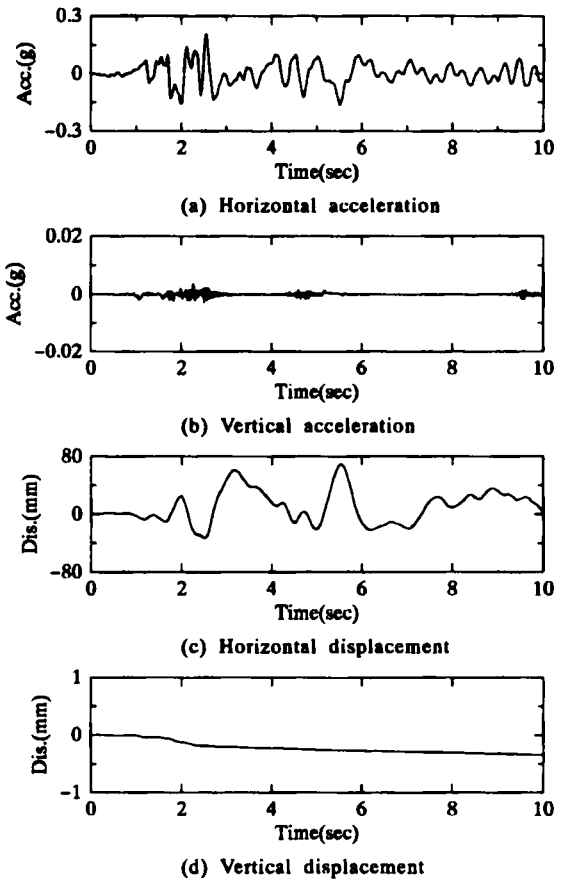

Figure 11. Seismic responses of 2-D shear column

Moreover, although the numerical damping and the Rayleigh damping are usually used in non-linear dynamic analyses of two-phase media, they are not considered in the following two examples in order to avoid their effects.

Seismic response analyses of saturated elastic soil deposits. As the first example of this type problem, we assume that soil deposits are isotropic and linear elastic. Soil parameters for analyses are given as: $G = 2{\cdot}4 \times 10^4$ kPa; $v = 0{\cdot}25$; $n = 0{\cdot}3$; $\rho = 1{\cdot}7\ t/m^3$; $\rho_f = 1{\cdot}0\ t/m^3$; $k = 1.0 \times 10^{-4}$ m/s; $\alpha = 1{\cdot}0$; $K_f = 2{\cdot}0 \times 10^6$ kPa.

Figures 8 and 9 show accelerations and displacements at a depth of 10 m in the 2-D shear column (reference) and the 2-D site model with absorbing boundaries, respectively. The excess pore water pressures at the corresponding depth in two types of models are shown in Figure 10. A comparison between Figures 8–10 indicates that the responses obtained by two types of models are completely consistent. Hence, the proposed absorbing boundary condition is appropriate for a linear elastic problem.

Seismic response analyses of saturated non-linear soil deposits. As the second example of this type of problems, we assume that soil deposits are non-linear and divided into two layers as shown in Figure 7. The basic parameters for the analyses are given as: $v = 0{\cdot}33$; $n = 0{\cdot}4$;

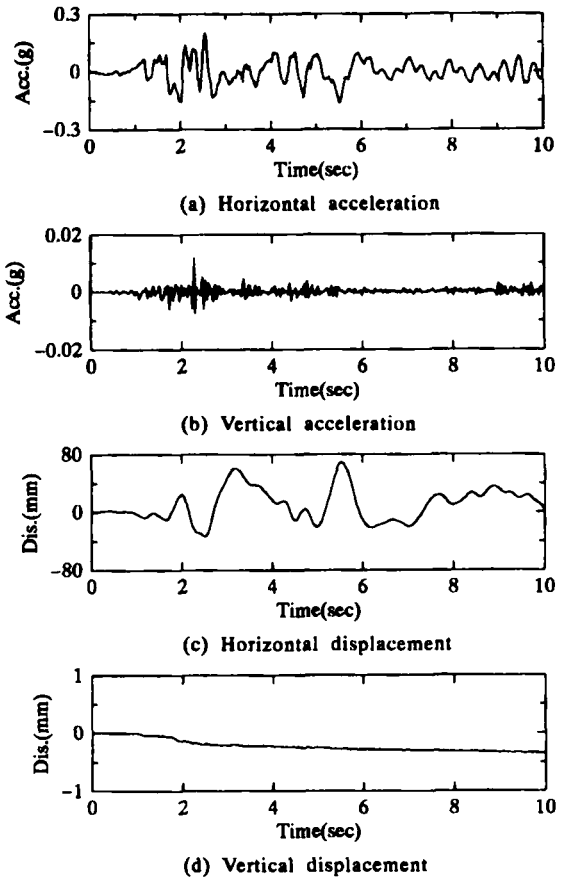

Figure 12. Seismic responses of 2-D site model at internal node A

$\rho = 1{\cdot}9\ t/m^3$; $\rho_f = 1{\cdot}0\ t/m^3$; $k = 1{\cdot}0 \times 10^{-5}$ m/s; $\alpha = 1{\cdot}0$; $K_f = 2{\cdot}0 \times 10^6$ kPa. The liquefaction parameters defined in the strain space multimechanism model are given in Table 1.

Figure 11 shows accelerations and displacements at a depth of 10 m in the 2-D shear column. The corresponding results at the internal node A and the boundary node B in the 2-D site model are shown in Figures 12 and 13, respectively. The excess pore water pressures in two types of model are presented in Figure 14. From these figures, it can be seen that a good agreement is obtained between the results at the internal node A in the 2-D site model and at the same depth in the 2-D shear column except for the vertical acceleration. Moreover, the results at the boundary node B in the 2-D site model are very consistent with those in the 2-D shear column except that the vertical components computed in the 2-D site model have a little oscillation due to the effect of reflected waves from the absorbing boundary (Figure 13). Hence, the proposed absorbing boundary condition is also appropriate for non-linear problems which include the non-linearity of soil in both near field and far field.

NUMERICAL ANALYSIS OF SATURATED SOIL–STRUCTURE SYSTEM

Now the proposed method is used to analyse a typical saturated soil–structure interacted problem as shown in Figure 15. Soil deposits are divided into two layers. The basic soil

Table I. Soil parameters for liquefaction analysis

Parameters	Upper layer	Lower layer
$G_{w0}(kPa)$	22990	65030
p_1	0·50	0·50
p_2	0·80	1·40
w_1	2·80	7·20
S_1	0·005	0·005
c_1	1·60	1·70
ϕ'_f	31°	37°
ϕ'_p	28°	28°
H_w	0·30	0·30

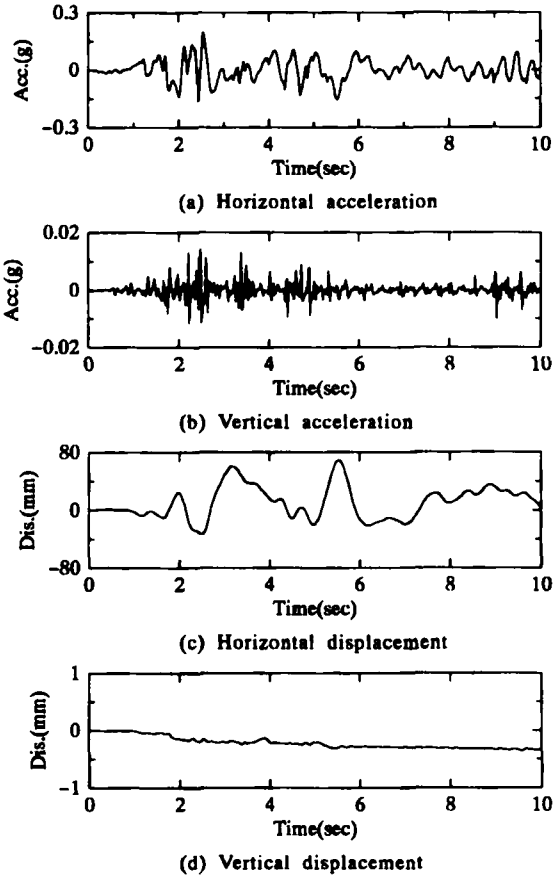

Figure 13. Seismic responses of 2-D site model at boundary node *B*

parameters and the liquefaction parameters are chosen as once given in the above example, i.e. the section *seismic response analyses of saturated non-linear soil deposits*. The structural parameters are given as: $G = 2{\cdot}0 \times 10^6$ kPa; $\nu = 0{\cdot}3$; $\rho = 0{\cdot}46$ t/m^3. The side boundaries are chosen as the proposed absorbing boundaries while the bottom boundary is assumed rigid and impervious.

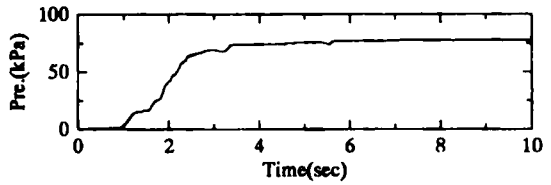

(a) 2D shear column

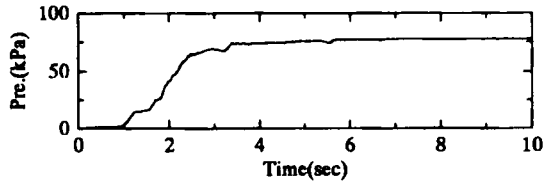

(b) At node A of 2D site model

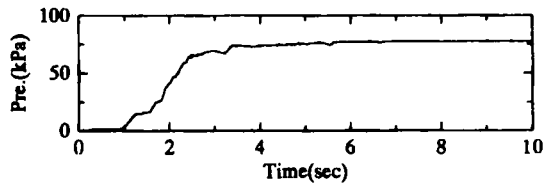

(c) At node B of 2D site model

Figure 14. Excess pore water pressures

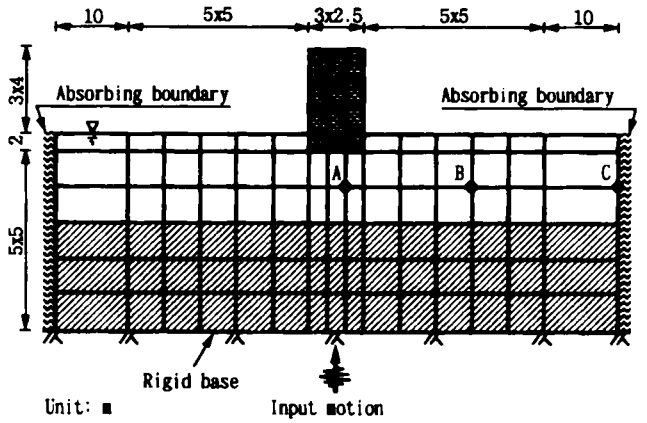

Figure 15. A FE model of typical saturated soil–structure system

The soil–structure system is subjected to the motion of the El Centro Earthquake (1940 NS) with a maximum acceleration of 0·2 g.

As the permeability of the soil is relatively small, the excess pore water pressure ratio can be defined by $1 - \sigma'_m/\sigma'_{m0}$. Figure 16 shows the contour diagrams for the excess pore water pressure ratio at the times of 4 and 10 s after excitation. The excess pore water pressure ratios in upper layer soil deposits are about 0·8 at the time of 10 s after excitation. Hence, the significant liquefaction takes place in this layer. The effect of the structure on the distribution of the excess

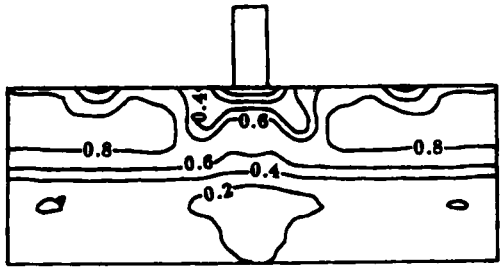

(a) At time of 4 seconds after excitation

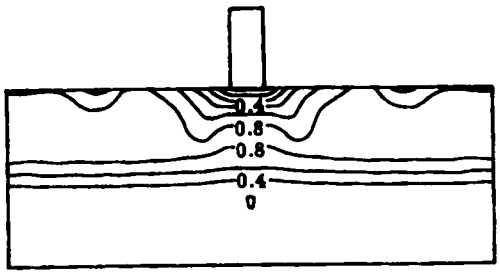

(b) At time of 10 seconds after excitation

Figure 16. Distributions of excess pore water pressure ratio

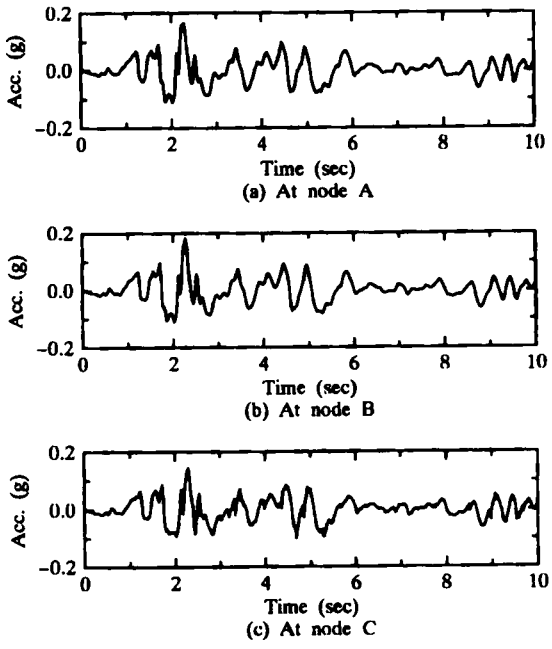

Figure 17. Horizontal accelerations

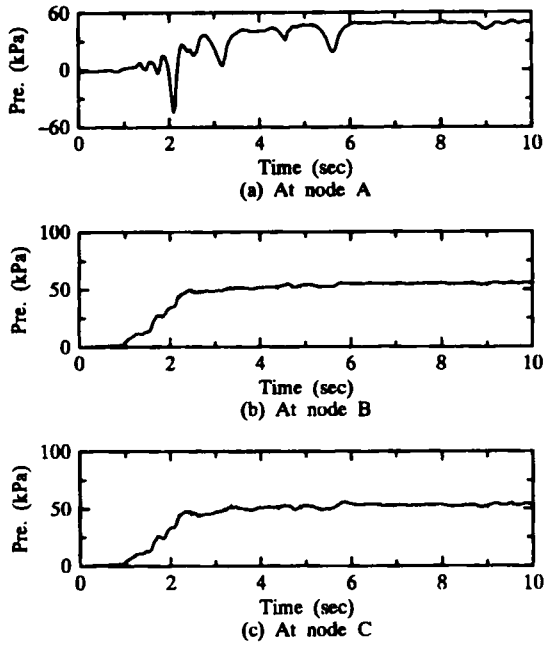

Figure 18. Excess pore water pressures

pore water pressure ratio can be seen by these contour diagrams, which indicate that such effect on the soil deposits is restricted within the zone near the structure after a significant liquefaction has taken place.

Figure 17 shows the time histories of horizontal accelerations at nodes *A*, *B* and *C*. Due to the effect of the structure, the maximum accelerations at nodes *A* and *B* are a little larger than the one at node *C*. Moreover, there exist some high frequency waves in the time history of acceleration at the boundary node *C*, which may be a result of spurious reflections at the absorbing boundary. The time variations of excess pore water pressures at the corresponding three nodes are presented in Figure 18. The excess pore water pressures at nodes *B* and *C* relatively far from the structure rapidly increase while at node *A* under the structure the high negative pore water pressure arises during the initial period of shaking due to the soil–structure interaction.

CONCLUSION

A non-linear seismic response analysis method for a 2-D saturated soil–structure system with an absorbing boundary is presented. Based on the 3-D strain-space multimechanism model for the cyclic mobility of sandy soil, the constitutive expression for the plane-strain condition is given. The simulation of the shaking table test shows that the proposed constitutive equation is capable of modelling the liquefication behaviour of sandy soil. Based on Biot's two-phase mixture theory, the finite element equation of motion for a saturated soil–structure system with an absorbing boundary during earthquake loadings is derived. By investigating numerical results of saturated soil deposits during earthquake loadings, the efficiency of the proposed absorbing boundary condition is proven. The proposed absorbing boundary condition can characterize reasonably

the effect of the far field. The numerical tests indicate that the proposed method is appropriate for not only linear problems but also severe non-linear problems such as the liquefaction of soil deposits. Moreover, a numerical seismic response analysis shows that the proposed method can provide relatively reasonable results for a saturated soil–structure system subjected to earthquake loadings.

ACKNOWLEDGEMENTS

The authors would like to thank the anonymous reviewers for their invaluable comments.

REFERENCES

1. M. A. Biot, 'Theory of propagation of elastic waves in a water-saturated porous solid. Part I: Low frequency range; Part II: Higher frequency range', *J. Acoust. Soc. Am.*, **28**, 168–191 (1956).
2. J. Ghaboussi and E. L. Wilson, 'Variational formulation of dynamics of fluid-saturated porous elastic solids', *J. Eng. Mech. Div. ASCE* **104**(4), 947–963 (1972).
3. O. C. Zienkiewicz and T. Shiomi, 'Dynamic behavior of saturated porous media: The generalized Biot formulation and its numerical solution', *Int. j. numer. anal. methods geomech.*, **8**, 71–96 (1984).
4. J. H. Prevost, 'Wave propagation in fluid-saturated porous media: An efficient finite element procedure', *Soil Dyn. Earthquake Eng.*, **4**, 183–202 (1985).
5. B. R. Simon, O. C. Zienkiewicz and D. K. Paul, 'Evaluation of u–w and u–π finite element methods for the dynamic response of saturated porous media using one-dimensional models', *Int. j. numer. anal. methods geomech.*, **10**, 461–482 (1986).
6. C. S. Desai and H. M. Galagoda, 'Earthquake analysis with generalized plasticity model for saturated soils', *Earthquake eng. struct. dyn.*, **18**, 903–919 (1989).
7. C. S. Desai and R. H. Gallagher, '*Mechanics of Engineering Materials*, Wiley, New York, 1984.
8. S. Iai, Y. Matsunaga and T. Kameoka, 'Strain space plasticity model for cyclic mobility', *Soils and Foundations*, **32**(2), 1–15 (1992).
9. T. Akiyoshi, H. Matsumoto, K. Fuchida and H. L. Fang, 'Cyclic mobility behavior of sand by the three dimensional strain space multimechanism model', *Int. j. numer. anal. methods geomech.*, **18**(6), 397–415 (1994).
10. H. L. Fang, 'Soil liquefaction during earthquakes and improvement effects by sand compaction piles', *Ph.D. Thesis*, Kumamoto University, Japan, 1995.
11. J. Lysmer andG. Waas, 'Shear waves in plane infinite structures', *J. Eng. Mech. Div. ASCE* **98**(1), 85–105 (1972).
12. J. Lysmer and R. L. Kuhlemeyer, 'Finite dynamic model for infinite media', *J. Eng. Mech. Div. ASCE*, **95**(4), 859–877 (1969).
13. W. D. Smith, 'A nonreflecting plane boundary for wave propagation problems', *J. Comp. Phys.*, **15**, 492–503 (1974).
14. F. Miura and K. Toki, 'Estimation of natural frequency and damping factor for dynamic soil structure interaction systems', *Proc. 3rd Int. Conf. Soil Dynamics and Earthquake Eng.*, Vol. 4, Prinston, 1987, pp. 738–87.
15. H. Modaressi and I. Benzenati, 'An absorbing boundary element for dynamic analysis of two-phase media', *Proc. 10th World Conf.* Balkema, Rotterdam, 1992, pp. 1157–1161.
16. G. Degrande and G. De Roeck, 'An absorbing boundary condition for wave propagation in saturated poroelastic media. Part I: Formation and efficiency evaluation', *Soil Dyn. Earthquake Eng.*, **12**, 411–421 (1993).
17. T. Akiyoshi, K. Fuchida and H. L. Fang, 'Absorbing boundary conditions for dynamic analysis of fluid-saturated porous media', *Soil Dyn. Earthquake Eng.*, **13**(6), 387–397 (1994).
18. Z. P. Bažant and B. H. Oh, 'Microplane model for progressive fracture of concrete and rock', *J. Eng. Mech. Div. ASCE* **111**(4), 559–582 (1985).
19. A. H. Stroud, *Approximate Calculation of Multiple Integrals*, Prencie Hall, Englewood Cliffs, N.J., 1971.